Effect of modifier cation field strength on the structures of magnesium oxide containing aluminoborosilicate glasses

Manzila Islam Tuheen, Jincheng Du*

Department of Materials Science and Engineering, University of North Texas, Denton, Texas

(*corresponding author. Email: jincheng.du@unt.edu)

Abstract

Network glass structures are commonly characterized by the network formers and their linkage but modifier can play an important role on various features of glass structures as well. In this work, we investigated the effect of cation field strength of common modifier cations with large difference of cation field strength on the structures of aluminoborosilicate glasses by performing molecular dynamics simulations with recently developed potentials. It was found that modifier cations with higher cation field strength such as Mg²⁺ significantly reduced the fraction of four-fold coordinated boron; suggesting cations with higher field strength favor non-bridging oxygen (NBO) generation in the silicate network and are less effective for charge compensation. The findings from our MD simulations are compared with the results from NMR and Raman spectroscopy studies as well as other MD simulations. Insights of the cation field strength effect on glass structures and the structural role of Mg²⁺ ions are gained from these simulations results and discussions.

Introduction

Multicomponent borosilicate and aluminoborosilicate glasses are of great significance in industrial and technological applications. First invented by the German glassmaker Otto Schott in 19th century, the use of borosilicate glasses started from kitchenware, thermometer but later expanded to sealing glasses, insulation fiber, heat and chemical resistant containers ^{1–7}. This family of glasses has also gained significant interest because of their applications in biomedicine ^{1,8} and nuclear waste immobilization ^{9–16}. The chemical durability and mechanical

properties of borate-glasses can further be enhanced by the introduction of Al₂O₃ in the borosilicate matrices therefore giving rise to aluminoborosilicate glasses ^{17–19}. The structures of oxide glasses consist of network made up of glass former oxides such as SiO₂, B₂O₃, and P₂O₅ that form the backbone of the glass, while the modifier oxides such as alkali and alkali earth oxides break up the network and form non-bridging oxygen (NBO)²⁰. Depending on the glass formation theory, the glass former oxides have higher cation-oxygen single bond strength or higher cation field strength than the modifier oxides. Some oxides such as alumina and lead have single bond strength or cation field strength between the former or modifier oxides. These oxides are called intermediate and these can play the role either as a former or modifier depending on the glass compositions. When modifiers are added to silicate glasses, they depolymerize the silicon-oxygen network made up of SiO₄ tetrahedrons by breaking the Si-O-Si linkages and formation of NBOs. The addition of modifier to borate or borosilicate glasses lead to conversion of three-fold coordinated boron ([3]B) to four-fold coordinated boron ([4]B) and instead of creating NBOs the modifier cations serve as local charge compenstator to negative charged [4]B groups²¹. The non-linear change of boron coordination as a function of modifier addition is known as boron anomaly which reflected in several properties such as density, glass transition temperature, and elastic moduli and was confirmed to be due to boron coordination change by solid state NMR^{22–25}. Addition of modifiers to aluminosilicate glasses have similar effect: modifier cations initially serve as charge compensators to negatively charged [4]Al units instead of creation of NBOs. The effect of addition of modifiers to aluminoborosilicate glasses becomes more complicated as there exist a competition of [4]Al and [4]B for modifier cations for charge compensation^{21,26–30}. It is generally believed that modifier cations first charge compensate ^[4]Al then [4]B, but the exact nature is still need to be studied. The simple picture of a modifier cation to either serve as a charge compensator or to create NBOs is further complicated by observations that cations with different field strength can behave differently in modifying the aluminosilicate or boroaluminosilciate network structures. For example, as compared to Na₂O and CaO, due to the smaller ionic radius and consequently higher field strength Mg²⁺, some consider MgO plays the role of an intermediate, i.e. can be a modifier or former depending on the glass composition.³¹ MgO is also considered to affect the aluminosilicate³¹ and borosilicate³² network structure differently as compared to other modifier cations. Despite these observations, the exact nature of these changes is still not clear. The goal of this work is to use a set of well-designed

aluminoborosilicate glass compositions with various mixing of the modifiers with different field strength to understand their structural role in these network glass structures.

When multiple glass formers and modifiers are present in a system, each element tends to compete for certain preferred site and coordination state to lower the total free energy of the system. Cation field strength (CFS) is one of the most important factors which control this ordering process in the glass, as shown CFS as a way to classify oxides as formers, intermediate or modifiers³³. One common definition of CFS is the ratio of the formal charge of the cation to the cation-oxygen bond distance squared. It is observed that, cations with higher field strength tend to promote the formation of five-fold coordinated Al and three-fold coordinated B^{21,32–35}. By performing NMR study on series of Mg, Ca, Sr, Ba, K, Na containing aluminoborosilicate glasses, Yamashita et al. ³⁶ reported that, for a given Al/B ratio, cations with higher field strength (greater charge to radius ratio) result in rising amount of NBOs and a reduce in the boron N₄. As a consequence of cation field strength, mixed modifier effect (MME) becomes operational ^{37,38}. MME it can be defined as the non-linear variation of glass properties with gradual substitution of certain metal ions ³⁹. These glass properties are associated with the ionic mobility of different pairs such as alkali/alkali, alkali-alkaline earth or alkaline earth/alkaline earth ³⁸. Wu and Stebbins ^{28,33} linked the rise of NBOs to the conversion of boron coordination through the structural reaction:

$$^{[4]}B \leftrightarrow ^{[3]}B + NBO$$
 (1)

When there is a higher content of the modifier, this equilibrium shifts to the right to avoid formation of linkages such as ^[4]B-O-^[4]B which are energetically less favorable. These increased NBOs dilute the glass network and stabilize the cation with higher field strength in the melt.

Magnesium oxide is a common compounds in silicate-melts of magma^{40,41}. It is also used in bioactive glass for bone repair owing to its ability to early stage apatite formation and to generate contact with living tissue^{42,43}. Glass properties such as viscosity, glass transition temperature, mechanical and chemical durability can be altered by the presence of MgO in the glass matrix^{44,45}. The role of Mg²⁺ ions in the glass matrix depends largely on the glass composition. It is generally considered as a glass modifier, but there are several studies suggesting its role as an intermediate^{46–49}. Along with its complex nature in the glass matrix, it interacts with other various cations differently. As a result, these systems are not easily

understood. Therefore, studies are yet to be performed to establish link among the different phenomena occurring in such systems.

Atomistic simulation methods such as molecular dynamics (MD) simulations is an effective tool in investigating the structures and structure-property relations of multicomponent oxide glass systems, given there are well developed interatomic potentials 50. Recent active developments have led to several available interatomic potentials for the simulations of borosilicate and aluminborosilicate glasses 51–55. Some of these potential sets adopted the idea of composition dependence boron charges and/or parameters to describe boron coordination change with composition while others adopt a fixed charge and parameter approach. Comparative studies of number of such potentials to evaluate their effectiveness have been established 30,56. In this work, a series of aluminoborosilicate glasses with fixed glass former percentage but different mixing of modifier cations with different field strength have been studied using MD simulations with the recent developed composition dependent partial charge potentials 52. The obtained results are compared with experimental findings from NMR and Raman spectroscopy 32, as well as with results from other MD simulations 55 to discuss the effect of CFS on the glass structures and the structural role of MgO in these glasses.

Methodologies and Simulation Details

Classical molecular dynamics (MD) simulations are used to study the structures of a series of borosilicate glasses designed with mixing of various modifier cations. The interatomic interactions among the atoms are described by the Born model of solids. They consist of short-range interactions in the Buckingham form and long-rage Coulombic interaction term with partial atomic charges. The total energy of the system can be expressed in Eq.2.

$$V(r_{ij}) = \frac{z_i z_j e^2}{4\pi\varepsilon_0 r_{ij}} + A_{ij} \exp(-r_{ij}/\rho_{ij}) - C_{ij}/r_{ij}^6 \quad (2)$$

Where r_{ij} stands for the interatomic distance between two ions i and j; e is electric charge, ε_0 is the permittivity of vacuum, A, ρ , and C are the different parameters for Buckingham term. In the Coulombic part of the potential, partial but constant charges of the ions are applied to better describe the partial covalent-ionic nature of the chemical bonds present in these systems. Table 1 lists the partial charges of the ions and the Buckingham term related parameters, where the A parameter for the B-O interaction is composition dependent 52,57. This set of composition

dependent boron potential has shown to be able to reproduce boron coordination change in wide composition ranges³⁰. Additionally, there are compatible parameters for all the oxides including MgO^{52,58}, which led us to use this set of potential in our MD simulations. To predict correct trajectories and melt structure at high temperature, there is a correction term at short interatomic distances were included in this potential set ⁵⁹. This empirical potential has been successfully used in diverse multi-component glass systems and efficiently derived the structures and properties ^{30,60–66}.

MD simulations were performed to generate the glass structures with compositions shown in Table 2 with a simulated melt and quench process by using the DL POLY 2.20 software package developed by Smith and Forester at Daresbury Laboratory UK⁶⁷. For short range interactions, the cut-off distance remained to be 8 Å. Long-range interactions were calculated using Ewald summation method where a relative precision of 1x10⁻⁶ and a cut-off distance of 10 Å were used. The equations of motion were integrated by Verlet Leapfrog algorithm with a time step of 1fs. To generate the initial glass structure, atoms were put in a cubic box randomly which is called simulation cell. In this work, each simulation cell contains ~10,000 atoms with such an initial box dimension to replicate the theoretical densities of the corresponding glass compositions. These initial configurations were then subjected to a simulated melt-quench process ⁶⁸. In this process, each randomly generated initial glass structure was energy minimized at 0K and relaxed at 300K followed by a heating up to 6000K to obtained fully liquefied uniform melt. The molten glass was then cooled down under a combination of constant volumetemperature (NVT) and constant volume-energy ensemble with a nominal cooling rate of 5K/ps. When the glass-melt reaches 300K, simulated glass structures were subjected to isobaric and isothermal step (NPT) to release any pressure. At the final temperature (300K) and pressure (1 atm), for every 50 configurations of the last 40,000 steps the trajectory was recorded and this MD simulated final structure was used to do the short- and medium-range structure analysis of the glasses. The structural analysis such as the pair distribution functions (PDF), coordination number (CN), bond angle distribution (BAD) and Q_n distribution were performed adopting the method described by Deng and Du²⁹. The cut-off distances for different pairs used in process of analysis were determined from the value of the first minima in the plots of partial total correlation functions.

Results

Partial total correlation functions and bond distances

Partial total correlation functions (T(r) = $4\pi r \rho(r)$, $\rho(r)$ is the number density) of the cation-oxygen pairs in the N8M19 glass composition are shown in Figure 1 as characteristic of the simulated glass series. The peak position of each of the plot indicates the bond distance of the corresponding cation-oxygen pairs. The bond distances of different cation-oxygen pairs are presented in Table 3 and these values are quite close to the respective experimental findings for most of the cation-oxygen pairs. Si-O peak is narrow and intense designates a well-defined silicon tetrahedron with its peak located around 1.61Å. This value is similar to the ones obtained by X-ray absorption spectra of silicate glass by Greaves et al.⁶⁹ and with other MD simulations and ab initio findings ^{30,70}. Al-O bond distances is ~1.77Å which is also close to the value obtained by EXAFS and XANES study of alkali aluminosilicate glasses by McKeown et al.⁷¹ and MD simulations of aluminoborosilicate and aluminophosphate glasses^{30,66}. B-O peak can be deconvoluted to two peaks – the peak at shorter distance (~1.41Å) indicates three-coordinated boron, [3]B and the peak at longer distance (~1.52Å) is resulted from four-coordinated boron, [4]B. Both of these values for in accordance with the findings from neutron diffraction of alkali borate melts⁷² and simulations of borosilicate and aluminoborosilicate glasses ⁵². Na-O bond distance varies from 2.40Å to 2.47Å depending on the glass compositions and similar results are obtained from experimental methods^{73,74}. Mg-O bond distance is around ~1.97Å most of the glasses which is lower than the value (~2.00Å) obtained by X-ray diffraction outcome of Guignard and Cormier⁴⁸. On the other hand, Ca-O bond distance is found to be 2.41Å which is an overestimation of the experimental results (2.32-2.36Å) from X-ray diffraction of calcium aluminosilicate glasses^{75,76}.

Glass former cations coordination and local environments

Oxygen coordination state of the glass forming elements captures one of the most important short-range structure information of the glass matrix. Coordination number can be calculated by integrating the first peak of partial pair distribution function and can be formulated as $\int_0^{r_c} 4\pi r^2 \rho(r) dr$. The cut-off value, r_c for each pair can be obtained from the first minima of the corresponding T(r) curve. The average coordination numbers of the glass formers (Si, Al, and B) are listed in Table 4. For Si, Al, B, the cut-off values were taken to be 2.25 Å, 2.35 Å, and

1.85 Å respectively. Throughout the entire series, silicon is observed to be four-fold coordinated which indicates the tetrahedral glass forming units of silicon. This is similar to the finding from X-ray absorption and X-ray diffraction spectra of silicate rich glasses ^{64,69}. Average coordination of aluminum is ~4 similar to the observation from NMR and EXAFS studies^{21,73} but there are five- and six-fold aluminum as listed in Table 5. However, the amount of five-fold coordinated aluminum does not follow any particular trend. In contrast to N19M8, N19C8 produces more amount of ^[5]Al+^[6]Al species. NMR studies show that Al³⁺ in glasses of this series is mostly 4-fold coordinated except N0M12 which has 16% 5-fold and 6% 6-fold coordination. ³² MD simulations in this work thus were able to reproduce aluminum coordination in most compositions except N0M12, which has no Na₂O but 12 mol% MgO. Higher field strength of Mg²⁺ cations forces both Al³⁺ to higher coordination numbers. ³² Although boron coordination can be well reproduced in our simulations as shown below, the discrepancy between MD and experiment of aluminum coordination for N0M12 suggest the potential need improvement, especially in describing compositions without alkali oxides.

The average coordination of boron varies from 3.45 to 3.00 decreasing systematically with increasing Mg concentration in the glasses (from N26M0 to N0M12) (Table 4). Hence, there is a decrease in the four-coordinated boron with increasing Mg to Na substitution. Again, when compared between N19M8 and N19C8 glass compositions (Table 6), decrease in the four-coordinated boron is greater in Mg containing glass (~29.11%) than the Ca containing glass (~38.72%). These findings are similar to the previously conducted NMR studies by Wu and Stebbins ³⁴, Bisbrouck et al.³² and also by Backhouse et al.⁷⁸. Therefore, with higher field strength of the modifier cation, boron N₄ is decreasing (Na>Ca>Mg).

A comparison of the boron N₄ obtained by MD simulations using two different potential sets developed by Deng and Du⁵²and Wang et al.⁵³, Yun, Dell and Bray (YDB) model^{22,23}, and NMR study by Bisbrouck et al.³² are summarized in Table 7. It can be observed that, there are fairly large differences between to two sets of potentials in terms of boron N₄ values. It is worth mentioning, Deng and Du's potential was developed with composition dependent boron related parameter whereas Wang et al.'s potential has fixed parameters. When plotted against MgO/[MgO+Na₂O] ratio (Figure 2) along with the NMR results, boron N₄ obtained from the simulations using Deng and Du's potential better agreement with experimental data. On the other hand, MD simulations with Wang et al. potential set³⁵ significantly overestimate boron N₄ in all

that modified YDB model for aluminoborosilicate glasses^{29,79} predicts constant boron N₄ values for several of the compositions (Table 7) as the model assumes all alkali earth or alkali oxide modifier have the same effect of charge compensation and to convert ^[3]B to ^[4]B. (The boron N₄ value from YDB model calculated in ref.³⁵ show large variations, which might be due to wrong assumptions for compositions with alumina). This assumption is incorrect as found in recent NMR studies^{21,32}. However, although the composition dependent potential change B-O potential parameter based on YDB model, the potential was able to distinguish the effect of cations with different cation field strength. For example, for compositions with MgO to Na₂O substitution, the boron N₄ from simulations of this work show continuous decreases, consistent with NMR results³².

Bond angle distribution (BAD) is important short-range structure information. Figure 3 shows the bond angle formed inside glass forming polyhedrons. The peak position of O-Si-O BAD is around 108.7° which is similar to the value obtained by X-ray diffraction of amorphous and vitreous silica ^{23,80}. The BAD of O-Al-O shows peak at around 107.1° which is in accordance with the experimental findings from aluminosilicate and gallosilicate solidates⁸¹. Both of the values of O-Si-O and O-Al-O bond angle are close to optimal tetrahedral angle and indicate tetrahedral sites. BAD of O-Si-O is narrower and sharper than O-Al-O due to the higher field strength of Si⁴⁺ than Al³⁺ ion. In case of O-Al-O BAD, there is a shoulder around 90° for the N0M12 glass compositions. For O-B-O BAD, it consists of two peaks. The smaller angle peak is around 109.9° which results from the tetrahedrally connected four-fold coordinated boron (^[4]B) and the larger angle at around 120° occurs for triangular three-fold coordination (^[3]B). With increasing Mg in the glass composition (from N26M0 to N0M12), the peak intensity of tetrahedral boron (^[4]B) lessens consistently indicating the decline in boron N4. When compared between N19M8 and N19C8, M19C8 has higher intensity of tetrahedral boron than N19M8 which is also consistent with the trend of boron N4 reported in Table 6.

Local environment around the glass modifier cations

Figure 4 shows the bond angle distribution (BAD) of the glass modifiers with neighboring oxygen. The BAD of O-Na-O, O-Mg-O, O-Ca-O all have two peaks each—the smaller angle peak is resulted from the sharing of oxygen atoms within the same polyhedron, on the other hand

the larger angle occurs due to the sharing of non-bridging oxygen (NBO) atoms from two different polyhedrons⁸². Table 8 lists the average oxygen coordination of the glass modifiers. The average coordination number of Mg is ~ 4.21 and it increases with increasing Mg in the structure but least value is obtained in the simple ternary glass, A0B0. Figure 5 shows the distribution of the oxygen coordination around Mg ions in the simulated glass series. It can be observed that, more than half of the Mg is four-fold coordinated and rest of these ions are of three-, five-, and six-fold coordination. Tetrahedral Mg is in highest amount in ternary A0B0 glass composition whereas from N19M8 to N0M12, percentage of tetrahedral Mg decreases regularly with increasing amount of MgO in the structure. The coordination number of Ca is around 6.67 in the glass composition N19C8.

Oxygen speciation and glass former Q_n distribution

Non-bridging oxygen is the dangling oxygen which does not link two glass forming polyhedrons and it forms a weak bond between the glass former and modifier. On the contrary, bridging oxygen atoms make connection between two glass forming polyhedrons such as [SiO4] or [AlO4] etc. Percentages of non-bridging (NBO), bridging (BO), and tri-bridging oxygen (TBO) are listed in Table 9. The obtained values from this work are also compared to the NMR results reported by Bisbrouck et al.³². Percentage of NBO is in very much well accordance with the NMR result. In case of both of the methods, NBO increased with increasing Mg in the glass composition from N26M0 to N0M12.

Table 10 shows the Q_n distribution of the silicon network structure of the simulated glass compositions. It can be used to analyze the glass network structure. By the notation Q_n, it is the average number of bridging oxygen to a glass forming polyhedron that is referred. From N26M0 to N8M19 glass composition, a broader distribution of silicon Q_n can be observed with majority of Q₄ species and rest of these to be Q₂ and Q₃ species. In these compositions, percentage of Q₄ is not highly altered by the change in MgO or with MgO/[SiO₂+Al₂O₃+B₂O₃] ratio (Figure 6a). In N0M12 glass composition, there is a dramatic increase in the Q₄ species which is also evident from the oxygen speciation in Table 9. There is a higher amount of Q₄ in N19C8 than in N19M8 but overall Q_n species are not significantly affected by substitution of Mg to Ca (Figure 6b). Highest extent of depolymerization can be observed in the simple ternary glass A0B0. The high

amount of Si Q₄ in N0M12 is mainly due to the composition difference as it has higher alumina and boron oxide content as compared to other glass compositions (Table 2).

Discussions

1. General structure features of multicomponent borosilicate glasses

Molecular dynamics simulation is an effective tool to model and analyze the structures of multicomponent glasses. Success of any simulation methods is dependent on the choice of appropriate potential set. Thanks to recent active development from several groups around the world, there are several potential sets available to make the simulations of borosilicate and aluminoborosilicate glasses possible^{29,53,70,83–85}. In this work, we have simulated seven glass compositions with varying Na⁺, Mg²⁺, and one with Ca²⁺, while the aluminoborosilicate glass network components remain fixed to investigated the effect of the modifier field strength on the network and other structure features. The recently developed partial charge composition dependent boron potential⁵² was used for the simulations of this work due to the fact that compatible potential parameters for all the oxides including MgO have been developed and the potential set has shown good accuracy to reproduce the boron coordination change in wide composition ranges^{30,70}. It is worth noting that our earlier study has shown the structural features and properties of borosilicate are indeed system size and cooling rate dependent⁸⁶. In this study, a relatively large system size of around 10,000 atoms and a typical cooling rate of 5K/ps were chosen for MD simulations of the glass compositions. The effect of the cation field strength was studied in terms of the change in coordination of the glass formers specially boron N₄ and also on different short- and medium-range structure features. The results from our simulations are compared with those from recent experimental (NMR)³² and simulations³⁵. The results show that the oxygen coordination of Si⁴⁺ remained four-fold coordinated, not affected by the composition change. The average coordination number of Al³⁺ is close to four for all composition. There are small amount of five- and six-fold coordinated aluminum as well but, when compared to experimental data³², especially for the compositions with high amount of MgO, MD simulations showed less five- and six-fold coordinated Al³⁺. The average coordination of boron varied with glass composition and with increasing CFS, the fraction of boron N₄ decreased. MD simulation results of this work are in good agreement with experiments for boron N₄ (Figure 2 and Table 7)32. Another recent work used fixed parameter potentials which significantly overestimate the

boron N₄ as compared to the experiments (shown in Figure 2), confirming our choice of the potential for this study. The effect of CFS on boron coordination can also be observed from the change in peak intensity of O-^[3]B-O, O-^[4]B-O in Figure 3. Among the glass network modifiers, we had Na, Mg and Ca in the studied glass. Na-O and Ca-O bond distances are quite close but Mg-O has a shorter bond distance than these two due to the lower coordination number of Mg²⁺ ions.

2. Effect of cation field strength on boron coordination

Cation field strength can be calculated from the cation-oxygen bond distance from MD simulations or Shannon effective ionic radii based on the coordination from MD. Two definition of cation field strength (CFS) are frequently used in the literature: one is based on the cation formal charge to cation-oxygen bond distance squared (Eq. 3) and named as CFS. The other one is based on the ratio of cation formal charge and the ionic radius of the cation, which is named as CFS1 (Eq. 4).

CFS =
$$\frac{Z_M}{(r_{M-O})^2}$$
 (3)

$$CFS1 = \frac{Z_M}{r_M} (4)$$

In which Z_M is the formal charge of the cation, r_{M-O} is the bond distance between cation and oxygen, and r_M is the cation ionic radius.

The cation field strength of common alkali and alkali earth glass modifier are calculated based MD simulation results of this work and those from earlier works, as well as those from the Shannon's radii (shown in Table 9). The CFS calculated based on cation-oxygen bond length from MD and those based on Shannon's radii (according to coordination number from MD) are very similar. It can be seen that despite the difference of the values of the methods, cation field strength essentially follows the same sequence: $Mg^{2+} > Ca^{2+} > Li^+ \approx Ba^{2+} > Na^+ > K^+$. Here, Mg^{2+} has by far the highest field strength among the common modifier cations calculated. This explains its strong effect on modifying the glass network structures. Ca^{2+} field strength is also fairly high, but lower than Mg^{2+} and higher than Na^+ . There is an overall decrease in the boron N_4 with increasing CFS. As discussed above, for the studied glass compositions, CFS follows the sequence: $Mg^{2+} > Ca^{2+} > Na^+$. CFS significantly impacted boron N_4 as can be observed in Table 6. With increasing amount of Mg^{2+} in the structure, fraction of four-coordinated boron decreased. It

can be explained by taken into consideration of the reaction equilibria present in boron containing glass as shown in Eq. 1. Modifiers with higher CFS shifts this equilibria toward the right hand side and produces more NBOs which in turns helps the stabilization of the high field strength of the cations ^{21,34}. This phenomenon can also be explained by the poorer charge compensating ability of the modifiers by higher CFS ^{32,88}. Also, in these systems, modifiers with higher CFS tends to create more NBOs instead of low poorly charged BO which promotes the unfavorable linkages such as ^[4]B-O-^[4]B, hence shift the above mention reaction toward the right hand side.

The empirical potential used in this MD simulation was developed with composition dependent boron related parameter such as A_{B-O} in Eq. 2 ⁵². When compared to the fixed charge empirical potential, it can better reproduce the boron coordination changes with composition³⁰. As shown in Table 7, calculated boron N₄ values in this work are quite consistent with the NMR study ³² but the fixed parameter potential set by Wang et al.⁵³ overestimates the fraction of boron N₄ quite significantly. Therefore, the composition dependent potential set ⁵² we used can successfully capture the effect of CFS on the structure of these glasses. It is worth to point out that the current potential show some discrepancy on Al³⁺ coordination.

3. Mg²⁺ local environment and structural role of MgO

As an alkali earth oxide, MgO is commonly considered to be a glass modifier in silicate glasses but for some compositions it is considered to be an intermediate therefore it behaves quite differently as compared to other typical modifier oxides. This in large extend is due to the significantly higher CFS of Mg²⁺as compared to other typical modifier cations such as Na⁺ and Ca²⁺. In aluminosilicate glasses, it was considered that MgO promote the formation of higher coordinated Al and change the Al and Si network mixing³¹. In the aluminoborosilicate glasses studied in this work, Mg²⁺ has an average coordination of around 4.2, much lower than the coordination number of Na⁺ and Ca²⁺ which ranges from 6 to 7 in this glass series (Table 8). The distribution of the coordination number in Figure 5 shows that majority (60-90% depending on the composition) of Mg²⁺ions are in four-fold coordination. The Mg-O distance is around 1.98Å which is also lower than the 2.3-2.4 Å of Na-O and Ca-O bond distances. As a result of this, MgO behaves quite differently in terms of converting [3]B to [4]B and the formation of NBOs in the system. It is generally believed that Mg²⁺ is not as good a charge compensator for

tetrahedrally coordinated charged units such as ^[4]B or ^[4]Al, due to its high CFS. It instead prefers to break the Si-O-Si bond and form NBOs. Both effects led to a decrease of boron N₄ in glasses with increasing amount of MgO to Na₂O substitution as shown in Figure 2. Although the R and K values do not change in these glass systems, boron N₄ value decreases. The trend from our simulation results is good agreement with experimental results based on NMR³². Comparing MgO and CaO, Mg²⁺ is responsible for the increase in the NBOs in the glass composition from N19M8 to N19C8 (Table 9). The work by Backhouse et al.⁷⁸ also showed that the presence of ^[4]Mg can reduce ^[4]B as compared to Ca²⁺ containing counterpart. The association of NBOs with Mg²⁺ ions is also confirmed by earlier experimental studiy³². It can be explained by the fact that, higher CFS of Mg²⁺ than Na⁺ or Ca²⁺ favors the creation of NBOs. So the results from MD simulations of this work suggest that Mg²⁺ ions have quite different local structures as compared to other typical modifier cations and they play different structural role, hence support the idea that it is an intermediate, between a modifier and a former.

Conclusions

In this work, a series of seven aluminoborosilicate glasses with varying amount of Na₂O, MgO and CaO have been studied to understand the effect of modifier cation field strength on the structures of these glasses using MD simulations. A partial charge pair-wise potential set with composition dependent boron related parameter was successfully used to generate the glass structures, with results consistent with recent experimental findings. It was found that, with increasing CFS of the modifier cations, the average boron coordination decreases. This can be explained by the preference of NBOs generation by high CFS modifier cations and, at the same time, a lesser capability of the higher CFS cations to play the role of charge compensators of the tetrahedrally coordinated charged groups (e.g. [BO₄]⁻ and [AlO₄]⁻). The results show that modifier CFS is an important consideration in designing glass compositions and understanding structure-property relations of glasses. The results also show the importance of using the suitable interatomic potentials to generate structures that are consistent with experiments for complex borosilicate and aluminoborosilicate glasses.

Acknowledgement

We would like to acknowledge support by US National Science Foundation (Project #1662288).

References

- 1. Yue Y, Tuheen MI, Du J. Borosilicate Glasses. In: *Encyclopedia of Materials:Technical Ceramics and Glasses*. Elsevier; 2021:1-21. doi:10.1016/B978-0-12-818542-1.00098-9
- 2. Donald IW. Preparation, properties and chemistry of glass- and glass-ceramic-to-metal seals and coatings. *J Mater Sci.* 1993;28(11):2841-2886. doi:10.1007/BF00354689
- 3. Fu Q, Rahaman MN, Fu H, Liu X. Silicate, borosilicate, and borate bioactive glass scaffolds with controllable degradation rate for bone tissue engineering applications. I. Preparation and in vitro degradation. *J Biomed Mater Res Part A*. 2010;95(1):164-171. doi:10.1002/jbm.a.32824
- 4. Phillips JC, Kerner R. Structure and function of window glass and Pyrex. *J Chem Phys*. 2008;128(17). doi:10.1063/1.2805043
- 5. Smedskjaer MM, Mauro JC, Youngman RE, Hogue CL, Potuzak M, Yue Y. Topological principles of borosilicate glass chemistry. *J Phys Chem B*. 2011;115(44):12930-12946. doi:10.1021/jp208796b
- 6. Smedskjaer MM, Youngman RE, Mauro JC. Principles of Pyrex® glass chemistry: Structure-property relationships. *Appl Phys A Mater Sci Process*. 2014;116(2):491-504. doi:10.1007/s00339-014-8396-1
- 7. Kato Y, Yamazaki H, Watanabe T, Saito K, Ikushima AJ. Early stage of phase separation in aluminoborosilicate glass for liquid crystal display substrate. *J Am Ceram Soc*. 2005;88(2):473-477. doi:10.1111/j.1551-2916.2005.00079.x
- 8. Lu X, Deng L, Kuo P-H, Ren M, Buterbaugh I, du J. Effects of boron oxide substitution on the structure and bioactivity of SrO-containing bioactive glasses. *J Mater Sci*. Published online 2017. doi:10.1007/s10853-017-0836-9
- 9. Gin S, Abdelouas A, Criscenti LJ, et al. An international initiative on long-term behavior of high-level nuclear waste glass. *Mater Today*. 2013;16(6):243-248. doi:10.1016/j.mattod.2013.06.008
- 10. Weber WJ, Ewing RC, Angell CA, et al. Waste and Plutonium Disposition. *J Mater Res*. 1997;12(8):1946-1978. doi:10.1089/ars.2013.5575
- Raj K, Kaushik CP. Glass matrices for vitrification of radioactive waste An update on R
 D efforts. *IOP Conf Ser Mater Sci Eng.* 2009;2. doi:10.1088/1757-899X/2/1/012002

- 12. Ojovan MI, Batyukhnova OG. Glasses for Nuclear Waste Immobilization. *WM '07 Conf.* 2007;(November):15.
- 13. Lee WE, Ojovan MI, Stennett MC, Hyatt NC. Immobilisation of radioactive waste in glasses, glass composite materials and ceramics. *Adv Appl Ceram*. 2006;105(1):3-12. doi:10.1179/174367606X81669
- 14. Ojovan MI, Lee WE. Chapter 17 Immobilisation of Radioactive Wastes in Glass. In: Ojovan MI, Lee WE, eds. *An Introduction to Nuclear Waste Immobilisation*. Elsevier; 2005:213-249. doi:https://doi.org/10.1016/B978-008044462-8/50019-3
- Goel A, McCloy JS, Pokorny R, Kruger AA. Challenges with vitrification of Hanford High-Level Waste (HLW) to borosilicate glass – An overview. *J Non-Crystalline Solids* X. 2019;4(August):100033. doi:10.1016/j.nocx.2019.100033
- 16. Grambow B. Nuclear waste glasses How durable? *Elements*. 2006;2(6):357-364. doi:10.2113/gselements.2.6.357
- 17. Sun T, Xiao H, Guo W, Hong X. Effect of Al2O3 content on BaO-Al2O3-B2O3-SiO2 glass sealant for solid oxide fuel cell. *Ceram Int*. 2010;36(2):821-826. doi:10.1016/j.ceramint.2009.09.045
- 18. Van Iseghem P, Amaya T, Suzuki Y, Yamamoto H. The role of Al2O3 in the long-term corrosion stability of nuclear waste glasses. *J Nucl Mater*. 1992;190(C):269-276. doi:10.1016/0022-3115(92)90090-8
- 19. Rosales-Sosa GA, Masuno A, Higo Y, Inoue H. Crack-resistant Al2O3-SiO2 glasses. *Sci Rep.* 2016;6(April):1-7. doi:10.1038/srep23620
- 20. Zachariasbn WH. THE ATOMIC ARRANGEMENT IN GLASS. *J Am Chem Sc*. 1932;196(1):3841-3851.
- 21. Wu J, Stebbins JF. Effects of cation field strength on the structure of aluminoborosilicate glasses: High-resolution 11B, 27Al and 23Na MAS NMR. *J Non Cryst Solids*. 2009;355(9):556-562. doi:10.1016/j.jnoncrysol.2009.01.025
- 22. Dell WJ, Bray PJ, Xiao SZ. 11B NMR studies and structural modeling of Na2OB2O3SiO2 glasses of high soda content. *J Non Cryst Solids*. 1983;58(1):1-16. doi:10.1016/0022-3093(83)90097-2
- 23. Yun YH, Bray PJ. Nuclear magnetic resonance studies of the glasses in the system K2OB2O3P2O5. *J Non Cryst Solids*. 1978;30(1):45-60. doi:10.1016/0022-

- 3093(78)90055-8
- 24. Bouty O, Delaye JM, Peuget S. Europium Structural Effect on a Borosilicate Glass of Nuclear Interest. *Procedia Chem.* 2012;7:540-547. doi:10.1016/j.proche.2012.10.082
- 25. Zhong J, Wu X, Liu ML, Bray PJ. Structural modeling of lithium borosilicate glasses via NMR studies. *J Non Cryst Solids*. 1988;107(1):81-87. doi:10.1016/0022-3093(88)90096-8
- 26. Du LS, Stebbins JF. Network connectivity in aluminoborosilicate glasses: A high-resolution 11B, 27Al and 17O NMR study. *J Non Cryst Solids*. 2005;351(43-45):3508-3520. doi:10.1016/j.jnoncrysol.2005.08.033
- 27. Huang Q, Liu J, He X, Liu T, Lu A. Analysis of structure evolution and performance in alkali-free glass substrates via XPS and infrared: Boron-aluminum anomaly. *J Non Cryst Solids*. 2021;555(August 2020). doi:10.1016/j.jnoncrysol.2020.120531
- 28. Wu J, Stebbins JF. Quench rate and temperature effects on boron coordination in aluminoborosilicate melts. *J Non Cryst Solids*. 2010;356(41-42):2097-2108. doi:10.1016/j.jnoncrysol.2010.08.015
- 29. Deng L, Du J. Development of effective empirical potentials for molecular dynamics simulations of the structures and properties of boroaluminosilicate glasses. *J Non Cryst Solids*. 2016;453:177-194. doi:10.1016/j.jnoncrysol.2016.09.021
- 30. Tuheen MI, Deng L, Du J. A comparative study of the effectiveness of empirical potentials for molecular dynamics simulations of borosilicate glasses. *J Non Cryst Solids*. 2021;553(July 2020):120413. doi:10.1016/j.jnoncrysol.2020.120413
- 31. Bechgaard TK, Scannell G, Huang L, Youngman RE, Mauro JC, Smedskjaer MM. Structure of MgO/CaO sodium aluminosilicate glasses: Raman spectroscopy study. *J Non Cryst Solids*. 2017;470(May):145-151. doi:10.1016/j.jnoncrysol.2017.05.014
- 32. Bisbrouck N, Bertani M, Angeli F, et al. Impact of magnesium on the structure of aluminoborosilicate glasses: A solid-state NMR and Raman spectroscopy study. *J Am Ceram Soc.* 2021;104(9):4518-4536. doi:10.1111/jace.17876
- 33. Wu J, Stebbins JF. Temperature and modifier cation field strength effects on aluminoborosilicate glass network structure. *J Non Cryst Solids*. 2013;362(1):73-81. doi:10.1016/j.jnoncrysol.2012.11.005
- 34. Wu J, Stebbins JF, Rouxel T. Cation Field Strength Effects on Boron Coordination in Binary Borate Glasses. *J Am Ceram Soc.* 2014;97(9):2794-2801. doi:10.1111/jace.13100

- 35. Bisbrouck N, Micoulaut M, Delaye J, et al. Influence of Magnesium on the Structure of Complex Multicomponent Silicates: Insights from Molecular Simulations and Neutron Scattering Experiments. 2021; 124: 11761-11776. doi:10.1021/acs.jpcb.1c06990
- 36. Yamashita H, Inoue K, Nakajin T, Inoue H, Maekawa T. Nuclear magnetic resonance studies of 0.139MO (or M' 2O)·0.673SiO2·(0.188 x)Al 2O3·xB2O3 (M = Mg, Ca, Sr and Ba, M' = Na and K) glasses. *J Non Cryst Solids*. 2003;331(1-3):128-136. doi:10.1016/j.jnoncrysol.2003.08.086
- 37. Wang X, Hu L, Meng X, Li H, Wang S. E ff ect of Al 2 O 3 and La 2 O 3 on structure and spectroscopic properties of Nd- doped sol gel silica glasses. *J Lumin*. 2018;204(August):554-559. doi:10.1016/j.jlumin.2018.08.015
- 38. Wang H, Hou X, Zhang Y, et al. The influence of the mixed alkaline earth effect on the structure and properties of (Ca, Mg)–Si–Al–O–N glasses. *Ceram Int.* 2021;47(9):12276-12283. doi:10.1016/j.ceramint.2021.01.078
- 39. Day DE. MIXED ALKALI GLASSES THEIR PROPERTIES AND USES. *J Non Cryst Solids*. Published online 1976:343-372. doi:10.1109/imtc.2005.1604557
- 40. Karki BB, Stixrude LP. Viscosity of MgSiO3 liquid at Earth's mantle conditions: implications for an early magma ocean. *Science*. 2010;328(5979):740-742. doi:10.1126/science.1188327
- 41. Stixrude L, Karki B. Structure and freezing of MgSiO3 liquid in Earth's lower mantle. *Science*. 2005;310(5746):297-299. doi:10.1126/science.1116952
- 42. Diba M, Tapia F, Boccaccini AR, Strobel LA. Magnesium-Containing Bioactive Glasses for Biomedical Applications. *Int J Appl Glas Sci.* 2012;3(3):221-253. doi:10.1111/j.2041-1294.2012.00095.x
- 43. Bellucci D, Veronesi E, Dominici M, Cannillo V. A new bioactive glass with extremely high crystallization temperature and outstanding biological performance. *Mater Sci Eng C*. 2020;110(January):110699. doi:10.1016/j.msec.2020.110699
- 44. Logrado M, Eckert H, Murata T, Nakane S, Yamazaki H. Structure-property relations in crack-resistant alkaline-earth aluminoborosilicate glasses studied by solid state NMR. *J Am Ceram Soc.* 2021;104(5):2250-2267. doi:10.1111/jace.17629
- 45. Bradtmüller H, Uesbeck T, Eckert H, Murata T, Nakane S, Yamazaki H. Structural Origins of Crack Resistance on Magnesium Aluminoborosilicate Glasses Studied by

- Solid-State NMR. *J Phys Chem C*. 2019;123(24):14941-14954. doi:10.1021/acs.jpcc.9b03600
- 46. Shimoda K, Tobu Y, Hatakeyama M, Nemoto T, Koji Saito K. Letter: Structural investigation of Mg local environments in silicate glasses by ultra-high field 25Mg 3QMAS NMR spectroscopy. *Am Mineral*. 2007;92(4):695-698. doi:doi:10.2138/am.2007.2535
- 47. Fiske PS, Stebbins JF. The structural role of Mg in silicate liquids: a high-temperature 25Mg, 23Na, and 29Si NMR study. *Am Mineral*. 1994;79(9-10):848-861.
- 48. Guignard M, Cormier L. Environments of Mg and Al in MgO-Al2O3-SiO2 glasses: A study coupling neutron and X-ray diffraction and Reverse Monte Carlo modeling. *Chem Geol.* 2008;256(3-4):111-118. doi:10.1016/j.chemgeo.2008.06.008
- 49. Pedone A, Malavasi G, Menziani MC. Computational insight into the effect of CaO/MgO substitution on the structural properties of phospho-silicate bioactive glasses. *J Phys Chem C*. 2009;113(35):15723-15730. doi:10.1021/jp904131t
- 50. Du J. Challenges in Molecular Dynamics Simulations of Multicomponent Oxide Glasses. Springer US; 2015.
- 51. Kieu LH, Delaye JM, Cormier L, Stolz C. Development of empirical potentials for sodium borosilicate glass systems. *J Non Cryst Solids*. 2011;357(18):3313-3321. doi:10.1016/j.jnoncrysol.2011.05.024
- 52. Deng L, Du J. Development of boron oxide potentials for computer simulations of multicomponent oxide glasses. *J Am Ceram Soc.* 2019;102(5):2482-2505. doi:10.1111/jace.16082
- 53. Wang M, Anoop Krishnan NM, Wang B, Smedskjaer MM, Mauro JC, Bauchy M. A new transferable interatomic potential for molecular dynamics simulations of borosilicate glasses. *J Non Cryst Solids*. 2018;498(December 2017):294-304. doi:10.1016/j.jnoncrysol.2018.04.063
- 54. Inoue H, Masuno A, Watanabe Y. Modeling of the structure of sodium borosilicate glasses using pair potentials. *J Phys Chem B*. 2012;116(40):12325-12331. doi:10.1021/jp3038126
- 55. Takada A, Catlow CRA, Price GD, et al. Related content Computer modelling of B 2 O 3.

 II . Molecular dynamics simulations of vitreous structures Computer modelling of Bz03:

- part 11. Molecular dynamics simulations of vitreous structures. Published online 1995.
- 56. Lee KH, Yang Y, Ziebarth B, Mannstadt W, Davis MJ, Mauro JC. Evaluation of classical interatomic potentials for molecular dynamics simulations of borosilicate glasses. *J Non Cryst Solids*. 2020;528. doi:10.1016/j.jnoncrysol.2019.119736
- 57. Du J, Cormack AN. Molecular dynamics simulation of the structure and hydroxylation of silica glass surfaces. *J Am Ceram Soc.* 2005;88(9):2532-2539. doi:10.1111/j.1551-2916.2005.00352.x
- 58. Sun W, Du J. Local ordering and interfacial structure between spinel crystal and aluminosilicate glasses from molecular dynamics simulations. *Int J Appl Glas Sci*. 2019;10(1):41-56. doi:10.1111/ijag.12554
- 59. Du J, Rene L. Compositional dependence of the first sharp diffraction peaks in alkali silicate glasses: A molecular dynamics study. 2006;352:3255-3269. doi:10.1016/j.jnoncrysol.2006.05.025
- 60. Xiang Y, Du J, Smedskjaer MM, Mauro JC. Structure and properties of sodium aluminosilicate glasses from molecular dynamics simulations. *J Chem Phys.* 2013;139(4). doi:10.1063/1.4816378
- 61. Du J, Cormack AN. Erratum: "The medium range structure of sodium silicate glasses: A molecular dynamics simulation" by J. Du and A.N. Cormack (Journal of Non-Crystalline Solids (2004) 349 (66-79) DOI:10.1016/j.jnoncrysol.2004.08.264). *J Non Cryst Solids*. 2005;351(10-11):956. doi:10.1016/j.jnoncrysol.2005.02.002
- 62. Du J, Cormack AN. The medium range structure of sodium silicate glasses: A molecular dynamics simulation. *J Non Cryst Solids*. 2004;349(1-3):66-79. doi:10.1016/j.jnoncrysol.2004.08.264
- 63. Ren M, Deng L, Du J. Bulk, surface structures and properties of sodium borosilicate and boroaluminosilicate nuclear waste glasses from molecular dynamics simulations. *J Non Cryst Solids*. 2017;476(May):87-94. doi:10.1016/j.jnoncrysol.2017.09.030
- 64. Lu X, Ren M, Deng L, Benmore CJ, Du J. Structural features of ISG borosilicate nuclear waste glasses revealed from high-energy X-ray diffraction and molecular dynamics simulations. *J Nucl Mater*. 2019;515:284-293. doi:10.1016/j.jnucmat.2018.12.041
- 65. Nienhuis ET, Tuheen M, Du J, McCloy JS. In situ pair distribution function analysis of crystallizing Fe-silicate melts. *J Mater Sci.* 2021;56(9):5637-5657. doi:10.1007/s10853-

- 020-05643-x
- 66. Tuheen MI, Du J. Structural features and rare earth ion clustering behavior in lanthanum phosphate and aluminophosphate glasses from molecular dynamics simulations. *J Non Cryst Solids*. 2022;578(December 2021):121330. doi:10.1016/j.jnoncrysol.2021.121330
- 67. Todorov I, Smith W, Cheshire U. The DL POLY 4 user manual. *STFC, STFC Daresbury* 2011;(January).
- 68. Pedone A. Properties Calculations of Silica-Based Glasses by Atomistic Simulations Techniques: A Review. Published online 2009:20773-20784.
- 69. Greaves GN, Fontaine A, Lagarde P, Raouxt D, Gorman SJ. Local structure of silicate glasses. *Nature*. 1981;293(October):611-616. doi:10.1038/293611a0
- 70. Fortino M, Berselli A, Stone-Weiss N, et al. Assessment of interatomic parameters for the reproduction of borosilicate glass structures via DFT-GIPAW calculations. *J Am Ceram Soc.* 2019;(June):7225-7243. doi:10.1111/jace.16655
- 71. Waychunas GA, Brown GE, Ponader CW, Jackson WE. Evidence from X-ray absorption for network-forming Fe2+ in molten alkali silicates. *Nature*. 1988;332(6161):251-253. doi:10.1038/332251a0
- 72. Majérus O, Cormier L, Calas G, Beuneu B. Temperature-induced boron coordination change in alkali borate glasses and melts. *Phys Rev B Condens Matter Mater Phys*. 2003;67(2):1-7. doi:10.1103/PhysRevB.67.024210
- 73. McKeown DA, Waychunas GA, Brown GE. Exafs and xanes study of the local coordination environment of sodium in a series of silica-rich glasses and selected minerals within the Na2OAl2O3SiO2 system. *J Non Cryst Solids*. 1985;74(2-3):325-348. doi:10.1016/0022-3093(85)90078-X
- 74. Walter SNH, Inman JM, Dent AJ, Greaves GN. Sodium and Silver Environments and Ion-Exchange Processes in Silicate and Aluminosilicate Glasses. *J Phys Chem Chem*. Published online 1993:9330-9336.
- 75. Cormier L, Neuville DR, Calas G. Structure and properties of low-silica calcium aluminosilicate glasses. *J Non Cryst Solids*. 2000;274(1):110-114. doi:10.1016/S0022-3093(00)00209-X
- 76. Petkov V, Billinge SJL, Shastri SD, Himmel B. Polyhedral units and network connectivity in calcium aluminosilicate glasses from high-energy x-ray diffraction. *Phys Rev Lett*.

- 2000;85(16):3436-3439. doi:10.1103/PhysRevLett.85.3436
- 77. Mozzi RL, Warren BE. The structure of vitreous boron oxide. *J Appl Crystallogr*. 1970;3(4):251-257. doi:10.1107/s0021889870006143
- 78. Backhouse DJ, Corkhill CL, Hyatt NC, Hand RJ. Investigation of the role of Mg and Ca in the structure and durability of aluminoborosilicate glass. *J Non Cryst Solids*. 2019;512(March):41-52. doi:10.1016/j.jnoncrysol.2019.03.003
- 79. Du L, Stebbins JF. Network connectivity in aluminoborosilicate glasses: 2005;351:3508-3520. doi:10.1016/j.jnoncrysol.2005.08.033
- 80. Grimley DI, Wright AC, Sinclair RN. Neutron scattering from vitreous silica IV. Time-of-flight diffraction. *J Non Cryst Solids*. 1990;119(1):49-64. doi:10.1016/0022-3093(90)90240-M
- 81. Borhade A V, Wakchaure SG. Synthesis and characterization of aluminosilicate and gallosilicate sodalites containing acetate ions. *Mater Sci.* 2011;29(2):127-134. doi:10.2478/s13536-011-0018-4
- 82. Xiang Y, Du J. Effect of strontium substitution on the structure of 45S5 bioglasses. *Chem Mater.* 2011;23(11):2703-2717. doi:10.1021/cm102889q
- 83. Kieu L-H, Delaye J-M, Cormier L, Stolz C. Development of empirical potentials for sodium borosilicate glass systems. *J Non Cryst Solids*. 2011;357(18):3313-3321.
- 84. Sundararaman S, Huang L, Ispas S, Kob W. New interaction potentials for borate glasses with mixed network formers. *J Chem Phys.* 2019;150(15). doi:10.1063/1.5079663.
- 85. Stevensson B, Yu Y, Edén M. Structure-composition trends in multicomponent borosilicate-based glasses deduced from molecular dynamics simulations with improved B-O and P-O force fields. *Phys Chem Chem Phys.* 2018;20(12):8192-8209. doi:10.1039/c7cp08593a
- 86. Deng L, Du J. Effects of system size and cooling rate on the structure and properties of sodium borosilicate glasses from molecular dynamics simulations. *J Chem Phys*. 2018;148(2). doi:10.1063/1.5007083
- 87. Moulton BJA, Picinin A, Silva LD, et al. A critical evaluation of barium silicate glass network polymerization. *J Non Cryst Solids*. 2022;583(December 2021):121477. doi:10.1016/j.jnoncrysol.2022.121477
- 88. Bunker BC, Kirkpatrick RJ, Brow RK. Local Structure of Alkaline-Earth Boroaluminate

Crystals and Glasses: I, Crystal Chemical Concepts—Structural Predictions and Comparisons to Known Crystal Structures. *J Am Ceram Soc.* 1991;74(6):1425-1429. doi:10.1111/j.1151-2916.1991.tb04123.x

Tables:

Table 1 Atomic charges and Buckingham potential parameters^{52,58}

Pairs	Aij (eV)	ρij (Å)	C_{ij} (eV.Å ⁶)	B_{ij} (eV.Å ⁶)	D_{ij}	n
O ^{-1.2} -O ^{-1.2}	2029.2204	0.343645	192.58	46.462	-0.32605	3.430
$Si^{2.4}$ - $O^{-1.2}$	13702.905	0.193817	54.681	28.942	-3.0250	3.949
$B^{1.8}$ - $O^{-1.2}$	Comp.dependent	0.171281	28.5	18.980	-4.1189	3.960
$Al^{1.8}$ - $O^{-1.2}$	12201.417	0.195628	31.997	51.605	-10.073	3.193
$Na^{0.6}$ - $O^{-1.2}$	4383.7555	0.243838	30.70	48.251	-4.7037	2.898
$Mg^{1.2}$ - $O^{-1.2}$	7063.4907	0.2109	19.210	54.077	-11.658	2.842
$Ca^{1.2}$ - $O^{-1.2}$	7747.1834	0.252623	93.109	74.737	-3.991	3.166

Table 2 Glass compositions, simulation cell size, experimental 32 and simulated densities of the simulated glasses (simulation cell $\sim 10,000$ atoms)

Glass		Composition (mol %)					Cell	Density	Density
							size	Exp33	MD
	SiO_2	B_2O_3	Al_2O_3	Na_2O	MgO	CaO	(Å)	(g/cm3)	(g/cm3)
N26M0	51.3	14.9	7.7	26.1	-	-	50.03	2.51	2.51
N19M8	51.2	14.9	7.7	18.7	7.5	-	50.35	2.45	2.46
N13M13	51.2	14.9	7.7	13.1	13.1	-	50.51	2.42	2.45
N8M19	51.2	14.9	7.7	7.5	18.7	-	50.53	2.41	2.45
N0M12	51.3	24.2	12.4	-	12.1	-	50.63	2.31	2.36
N19C8	51.2	14.9	7.7	18.7	-	7.5	50.25	2.51	2.52
A0B0	66.1	-	-	24.2	9.7	-	51.29	2.49	2.51

Table 3 Cation-oxygen bond distances in the simulated glass compositions and corresponding values from experimental methods

Glass	N26M0	N19M8	N13M13	N8M19	N0M12	N19C8	A0B0	Exp.
Si-O	1.61	1.61	1.61	1.61	1.61	1.61	1.61	1.60-1.61 ⁶⁹
Al-O	1.77	1.77	1.77	1.77	1.76	1.77	-	1.76^{73}
[3] B- O	1.42	1.41	1.41	1.41	1.36	1.41	-	$1.37 - 1.38^{72,77}$
${}^{[4]}B-O$	1.52	1.52	1.51	1.50	-	1.51	-	$1.48 - 1.49^{72,77}$
Na-O	2.43	2.46	2.47	2.47	-	2.45	2.40	$2.30 - 2.32^{74}$,
								$2.56 - 2.62^{73}$
Mg-O	-	1.96	1.97	1.97	2.01	-	1.98	2.00^{48}
Ca-O	-	-	-	-	-	2.41	-	$2.32 - 2.36^{75,76}$

Table 4 Average oxygen coordination number of the glass formers (Si, Al, and B)

Glass	Si	Al	В
N26M0	4.00	4.00	3.45
N19M8	4.00	4.00	3.29
N13M13	4.00	4.01	3.23
N8M19	4.00	4.02	3.17
N0M12	4.00	3.99	3.00
N19C8	4.00	4.03	3.39
A0B0	4.00	N/A	N/A

Table 5 Percentage of [4] Al, [5] Al, and [6] Al in the simulated glass series

Glass	^[4] A1	^[5] A1	^[6] Al
N26M0	99.53	0.47	0.000
N19M8	98.89	1.07	0.001
N13M13	99.29	0.66	0.050
N8M19	98.69	1.31	0.000
N0M12	96.78	1.19	0.003
N19C8	97.67	2.17	0.159
A0B0	N/A	N/A	N/A

Table 6 Percentage of ${}^{[3]}B$ and ${}^{[4]}B$ in the simulated glass series

Glass	$^{[3]}B$	$^{[4]}B$
N26M0	54.97	45.03
N19M8	70.89	29.11
N13M13	77.59	22.41
N8M19	83.26	16.74
N0M12	99.98	0.02
N19C8	61.28	38.72
A0B0	N/A	N/A

Table 7 Comparison of boron N_4 from this work (MD simulation and YDB), NMR study³², YDB from Bisbrouck et al.³⁵ and MD simulations using fixed parameter potential³⁵.

Glass	MD (This work)	YDB (This work)	NMR ³²	YDB ³⁵	MD - Fixed parameter potential ³⁵
N26M0	45.0	43.1	57	72	71.6
N19M8	29.1	42.8	37	71	64.6
N13M13	22.4	42.8	24	36	55.6
N8M19	16.7	42.8	7	0	48.1
N0M12	0.0	0.0	2	0	18.8
N19C8	38.7	42.8	46	71	69.9
A0B0	N/A	N/A	N/A	N/A	N/A

Table 8 Average coordination number of Na⁺, Mg²⁺, Ca²⁺

Glass	Na ⁺	Mg ²⁺	Ca ²⁺
(cut-off, Å)	(3.23)	(2.62)	(3.16)
N26M0	6.83	-	-
N19M8	6.78	4.17	-
N13M13	6.91	4.22	-
N8M19	6.92	4.24	-
N0M12	N/A	4.33	-
N19C8	6.87	-	6.67
A0B0	6.10	4.11	-

Table 9 Oxygen speciation in the simulated glass series

Glass	%NBO	%BO	%TBO	%NBO (NMR) ³²
N26M0	12.20	87.47	0.32	10
N19M8	14.87	84.55	0.56	13
N13M13	16.02	83.12	0.79	15
N8M19	17.03	81.59	1.20	18
N0M12	5.51	88.76	5.71	5
N19C8	13.41	85.97	0.63	12
A0B0	40.35	59.42	0.00	41

Table 10 Q_n distribution of the silicon glass network

Glass	O ₁	O ₂	O ₃	O ₄
N26M0	0.14	2.57	29.90	67.40
N19M8	0.51	4.06	32.00	63.43
N13M13	0.58	4.68	30.57	64.17
N8M19	0.51	5.30	28.82	65.37
N0M12	0.14	0.50	11.67	87.69
N19C8	0.20	3.15	29.75	66.90
A0B0	4.44	21.48	44.62	29.29

Table 11 Cation field strengths calculated from different formulations and cation radius and cation-oxygen bond distance from MD simulations

Cation	Li ^{+,*}	Na^+	$K^{+,*}$	Mg^{2^+}	Ca^{2+}	Ba ^{2+,*}
$r_{\text{M-O}}$ (Å, MD)	1.95	2.39	2.77	1.97	2.41	2.73
CFS (MD)	0.263	0.175	0.130	0.515	0.344	0.268
CN (MD)	3.5	7.0	7.8	4.2	6.7	7.5
$r_{\rm M}({\rm \AA,Shannon})^+$	0.59	1.00	1.51	0.57	1.00	1.42
CFS1 (Shannon)	1.69	1.00	0.66	3.51	2.00	1.41
(1 00	2.40	2.01	1.07	2.40	2.02
$r_{M-O}(A, Shannon)^+$	1.99	2.40	2.91	1.97	2.40	2.82
CFS (Shannon)	0.253	0.174	0.118	0.515	0.347	0.251

^{*} cation oxygen bond distance from earlier MD simulations 59,87

⁺ Shannon effective ionic radii based on the coordination number close to MD results, O²-radius is assumed to be 1.40 Å.

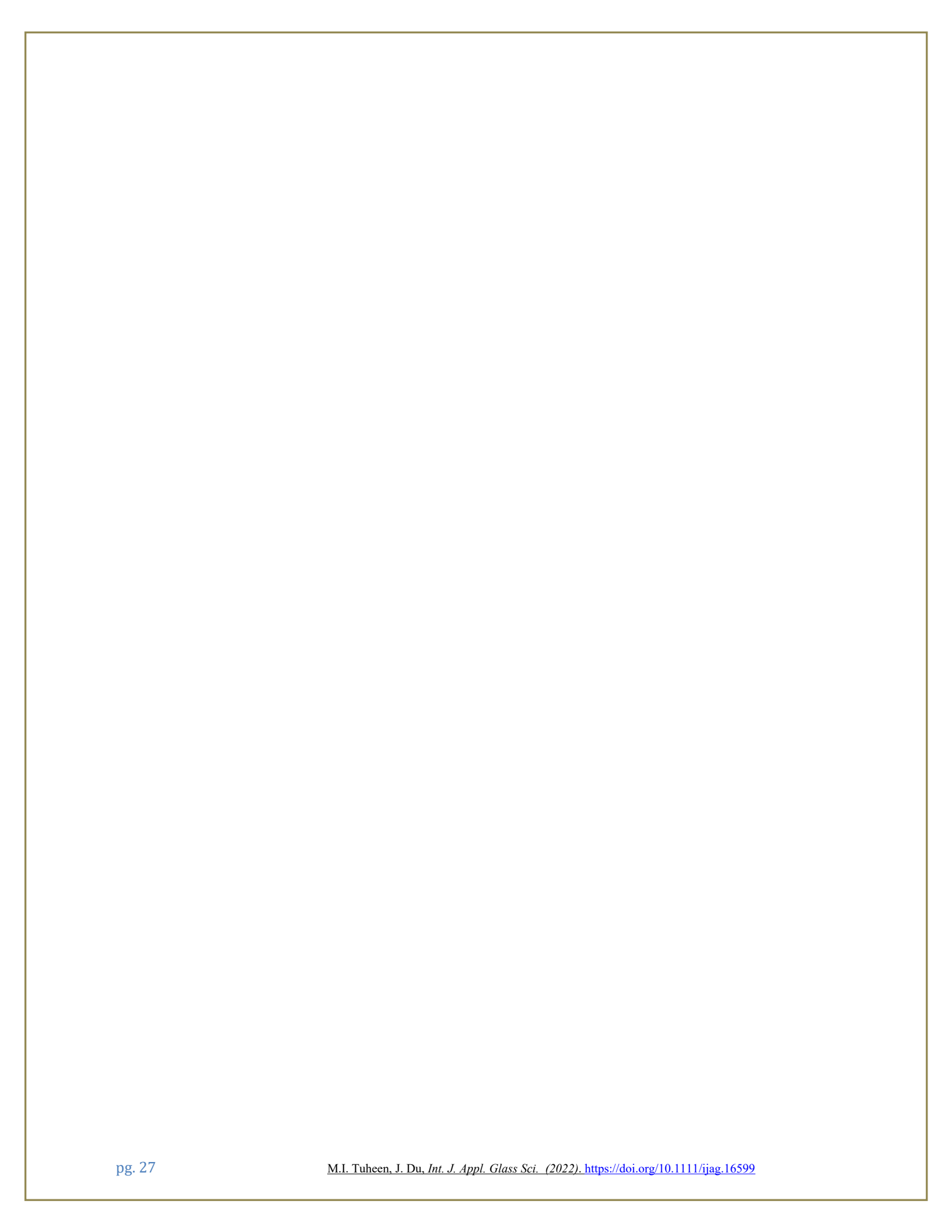


Figure Captions:

Figure 1 Partial total correlation function (T(r)) of the cation -oxygen pairs in simulated N8M19 glass composition

Figure 2 Comparison of born N₄ from (this work), fixed parameter potential³⁵ and NMR study³²

Figure 3 Bond angle distribution (BAD) of the glass formers with neighboring oxygen, a) O-Si-O, b) O-Al-O, c) O-B-O

Figure 4 Bond angle distribution of the glass modifier cations with neighboring oxygen. a) O-Na-O, b) O-Mg-O, c) O-Ca-O

Figure 5 Distribution of Mg coordination number in the simulated glass series

Figure 6 Q_n distribution of silicon glass network in the simulated glass series (a) MgO to Na₂O substitution and (b) MgO versus CaO

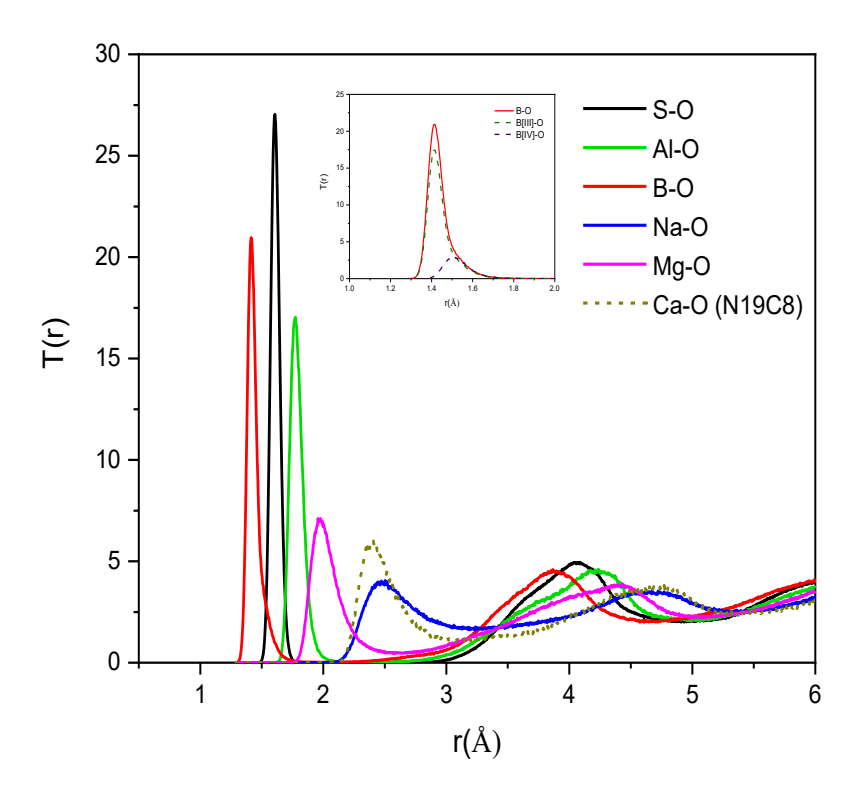


Figure 1

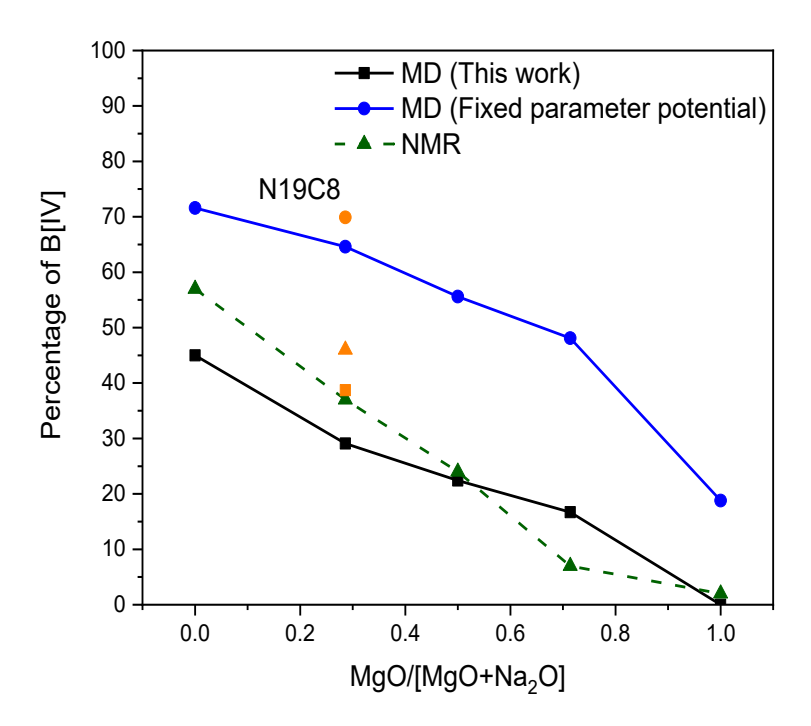
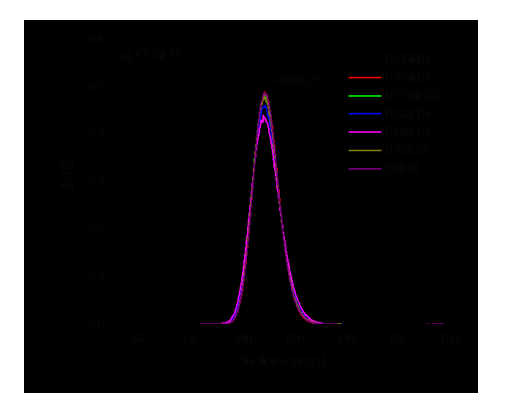
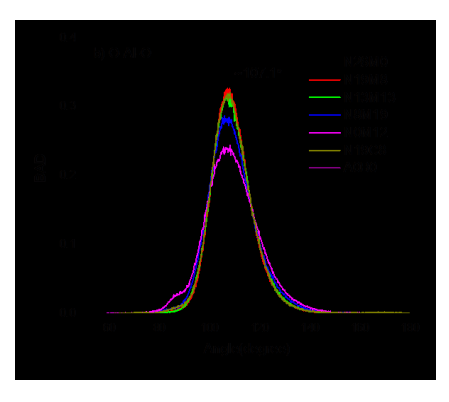


Figure 2





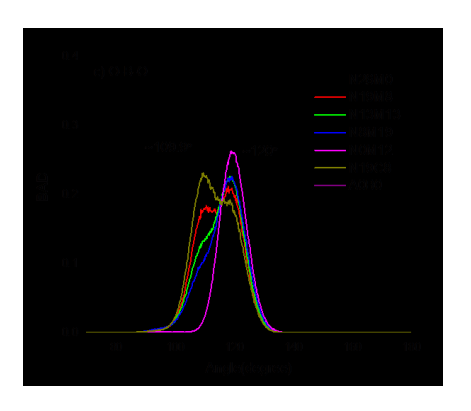
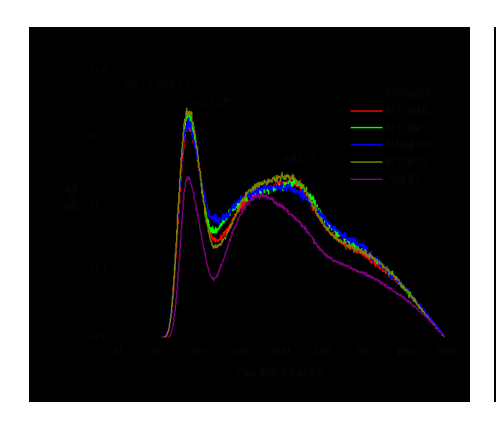
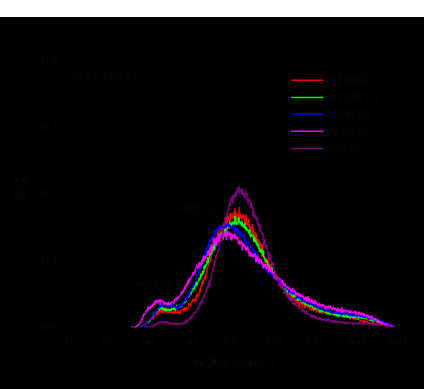


Figure 3





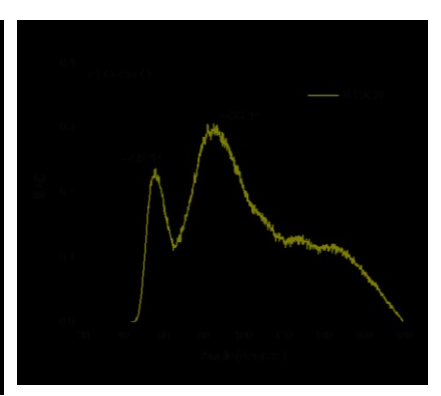


Figure 4

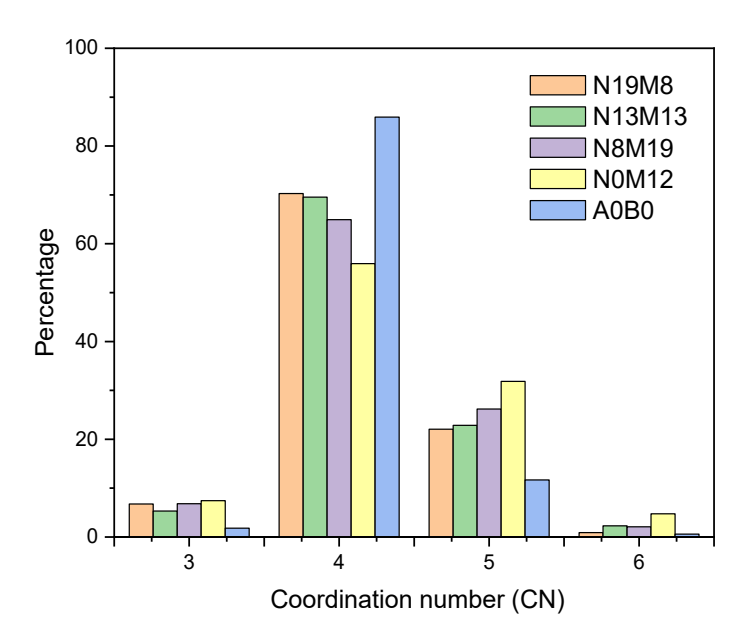


Figure 5

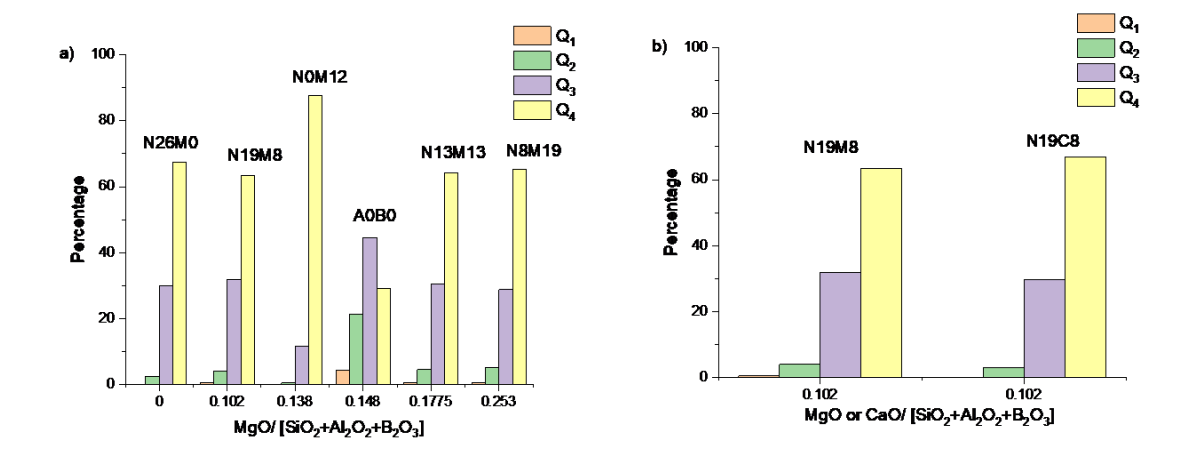


Fig. 6